Hot Formability of Particle reinforced Ti-Alloys.

Authors: C. Poletti[1], S. Kremmer[2]

1 Vienna University of Technology, Karlsplatz 13 / E308, A-1040 Vienna, Austria Tel: +43-1-58801-30813, e-mail: cpoletti@mail.zserv.tuwien.ac.at
2 BÖHLER Schmiedetechnik GmbH & CoKG, Mariazellerstrasse 25, A-8605 Kapfenberg, Austria, e-mail: sascha.kremmer@bohler-forging.com

Abstract

Titanium alloys exhibit mechanical and physical properties that fit structural applications demanding light-weight, corrosion resistance and biocompatibility. Ceramic reinforcements can further improve some of these mechanical properties, such as wear resistance, specific stiffness and specific strength. In comparison to continuous reinforced titanium alloys, the particle reinforced alloys (PRTi) do not show anisotropies and are cheaper in production. Furthermore, a potential production route by hot working is more feasible for PRTi.
The present work studies the mechanisms of hot deformation of the PRTi produced in-situ by powder metallurgy of Ti-6Al-4V-powders with additions of a certain amount of B and C. Thus, TiB precipitates form as ceramic reinforcements in the Ti-6Al-4V-0.1C matrix. Hot compression tests on this PRTi and on conventional Ti64 were carried out at temperatures between 850°C and 1100°C, and at strain rates of $0.001s^{-1}$ to $10s^{-1}$. The processing maps, which represent the efficiency of power dissipation as functions of strain rate and temperature at a chosen true strain value, were derived from flow curves produced by compression tests with the Gleeble®1500 device. These processing and instability maps are correlated to microstructural changes and compared with those of TiC-particle reinforced Ti662 produced by Cold-Hot Isostatic Pressing (CHIP). The mechanisms of energy dissipation by hot deformation are discussed.

1 Introduction

Titanium alloys show high specific mechanical properties up to elevated temperatures and also very good corrosion resistance, which makes them attractive not only for aerospace components, but also for automotive, industrial, medical and off shore applications [1,2]. The presence of ceramic reinforcement in such alloys can further improve some of their mechanical properties [3,4] and also the wear resistance, which is very poor in the case of titanium alloys in general [5]. An important disadvantage of such composite alloys is a lower ductility compared to titanium alloys.
There are two possible approaches of matrix reinforcement. On the one hand continuous monofilaments and fibres can be used to improve considerably the strength and the stiffness of titanium alloys in the direction of the monofilaments [2]. However, the fabrication of continuously reinforced materials is rather expensive. Further, it is not possible to use hot working processes for such alloys and their properties show rather large anisotropies. On the other hand, the particulate reinforced alloys are cheaper in production, show good potential to be hot-worked and machined, and their properties are more or less isotropic. According to previous works such particles that can be used for reinforcement purposes can be ceramics, oxides and intermetallic compounds

[6,7,8,9]. In the case of Ti/TiB composites the most common way of fabrication is an In-situ method, where TiB_2 and/or B are used as precursors. The resulting reinforcement particles always had the stoichiometric composition of TiB [10,11].
Reasons for choosing TiB and TiC for the production of particulate and whisker reinforced PRTi are their high Young's modulus, good chemical stability, low solid solubility and their coefficient of thermal expansion (CTE), which is similar to the matrix CTE [12]. The reinforcement of titanium alloys with 10vol % TiB results in an increment of the 0.2% proof strength of about 50% at 800°C and of 16% at room temperatures [13].
The objective of this work is to study the deformation behaviour of the composite material Ti-6Al-4V-1.0B-0.1C under compression at temperatures used for conventional Ti64 $\alpha + \beta-$ or $\beta-$forging and to obtain a first insight into the ongoing deformation mechanisms.
The hot deformation of those materials was analysed by correlating the measured flow data to the modified Dynamic Mechanical Model (DMM) developed by Murty and Rao [14] based on the DMM developed by Prasad et. al [15].
At any strain (ε) and temperature (T) the power (P) absorbed by the work piece during plastic flow can be divided into two components:

$$P = G + J = \int_0^{\dot{\varepsilon}} \sigma d\dot{\varepsilon} + \int_0^{\sigma} \dot{\varepsilon} d\sigma = \sigma\dot{\varepsilon} \qquad \textbf{Equation 1}$$

where $\dot{\varepsilon}$ is the strain rate, σ is the flow stress, G is the content and refers to the heat dissipation in the work-piece, and J is the co-content, which refers to microstructural transformations. The parameter of power dissipation defined as $\eta = 2J/P$, represents the relative rate of entropy production due to microstructural dissipation, i.e. the microstructural transformations within the material, such as recovery, recrystallisation, phase transformations and material damage [16]. From equation 1, η is calculated as:

$$\eta = \frac{2J}{P} = \frac{2(P-G)}{P} = 2\left(1 - \frac{\int_0^{\dot{\varepsilon}} \sigma d\dot{\varepsilon}}{\sigma\dot{\varepsilon}}\right) \qquad \textbf{Equation 2}$$

Because no experimental data can be obtained for a strain rate of 0, the integral to evaluate G can be calculated starting from a minimum strain rate:

$$G = \int_0^{\dot{\varepsilon}} \sigma d\dot{\varepsilon} = \int_0^{\dot{\varepsilon}_{min}} \sigma d\dot{\varepsilon} + \int_{\dot{\varepsilon}_{min}}^{\dot{\varepsilon}} \sigma d\dot{\varepsilon} = \left[\frac{\sigma\dot{\varepsilon}}{m+1}\right]_{\dot{\varepsilon}=\dot{\varepsilon}_{min}} + \int_{\dot{\varepsilon}_{min}}^{\dot{\varepsilon}} \sigma d\dot{\varepsilon} \qquad \textbf{Equation 3}$$

where m is the strain rate sensitivity. The value of m for the first integral is estimated as the slope of the curve $\log \sigma$ versus $\log \dot{\varepsilon}$ near $\dot{\varepsilon}_{min}$. The strain rate sensitivity from $\sigma = K\dot{\varepsilon}^m$ can vary from 0 (ideal non-dissipator material) to 1 (ideal dissipator).
Finally, flow instability is predicted in the modified DMM when the instability parameter $\kappa < 0$:

$$\kappa = \frac{2m}{\eta} - 1 < 0 \qquad \textbf{Equation 4}$$

A good hot formability of the material is indicated by high values for the power dissipation and the presence of stability in the flow behaviour at a desired temperature and strain rate.

2 Experimental

The material investigated were cylindrical billets of Ti-6Al-4V-1.0B-0.1C produced by Cold-Hot Isostatic Pressing (CHIP). From these billets cylindrical samples of 10 mm diameter and 15 mm in length were fabricated by an erosion process.
Compression tests at 850, 900, 950, 1010, 1050 and 1100°C and at 0.001-0.01-0.1 and $1s^{-1}$ were performed using a Gleeble®1500 machine and at 10 s^{-1} a Gleeble®3600 was applied. These systems work with a servo-hydraulic mechanism for applying the desired compression force during an electrical heating by the ohmic resistance of the sample. The temperature was measured using a K-type thermocouple attached directly to the sample. In order to reduce the oxidation of the machine and the sample, the tests were carried out under argon atmosphere at low pressure. To reduce the barrelling of the sample as a consequence of the temperature gradient and the friction, a "sandwich" of graphite foil, colloidal graphite and Mo foil was used between the sample and the anvil. For measurements at highest strain rate a system of mechanical brakes is used to substitute servohydraulic braking. Due to the non-uniform deformation, transverse strain measurements (C-Gauge) were applied instead of the classic longitudinal strain measurement.
After deformation, the samples were air-cooled, cut through their axis parallel to the direction of compression, embedded, and finally ground and polished for metallographic investigations. The two phases of the Ti alloy (α = hcp and β = bcc) were distinguished using the Back Scattered Electron (BSE) mode in a Philips 30XL Scanning Electron Microscope (SEM). The contrast observed is due to the distribution of the alloying elements: Al-rich α-phase dark, and V-rich β -phase, denser than the α phase, appears bright. The TiB particles are darker (less dense) than the α phase.

3 Results and discussion

3.1 Microstructure

Estimating that all the Boron and the entire Carbon included in the material react with Ti to form TiB and TiC respectively, this would result in the presence of approximately 3vol% TiB and 0.15vol% TiC in the Ti-6Al-4V (Ti64) matrix. Thus, it is not possible to identify this small amount of TiC particles by SEM and EDX investigations. For comparison of reinforced and plain Ti64 microstructures, Ti64 samples produced by Dynamet applying the CHIP method were included in the characterization.
The microstructure of the as received samples is shown in Figure 1: in grey the β-phase, in dark grey the α-phase in black the TiB precipitates. The unreinforced Ti64 exhibits a lamellar microstructure with an average grain size of about 50-150µm, whereas the matrix of the TiB reinforced material shows a fine α–globular microstructure with grains of about 5-20µm. Two types of TiB precipitates can be observed: big isolated elongated particles between 5 and 20 µm long and 1 µm thick and small thin precipitates of 1-5µm in length appearing in a needle shape. Furthermore, the thin

needles are preferentially allocated along some prior β-grains, while big particles are located inside other prior β-grains.
The larger TiB particles are identified as primary TiB precipitates and the fine TiB whiskers as particles resulting from the eutectic reaction [17]. Both types of particles have an elongated morphology. However, by 3D reconstruction applied in [17] it was found, that the volume of the primary TiB particles is approximately an order of magnitude larger than that of eutectic TiB particles.

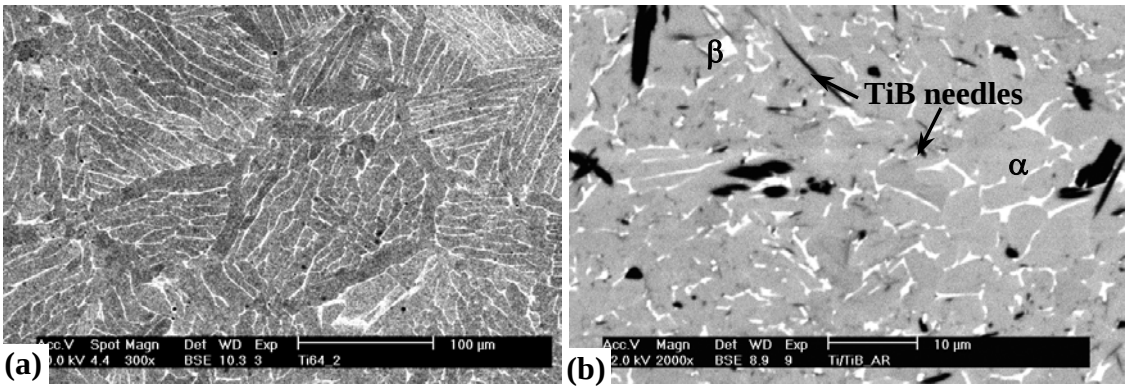

Figure 1: (SEM-BSE micrographs) As received samples a) unreinforced Ti64 showing large α-lamellae b)Ti64-PRTi with TiB particles and needles, and a fine globular substructure of the α-phase with β-phase at the boundaries.

After the compression tests, the samples were cooled in air. Therefore, the alpha content and its shape shown in the micrographs are not the same as those at test temperature immediately after deformation. Figure 2 - Figure 4 show the microstructures of TiB reinforced samples after deformation and air-cooling. The arrows indicate the load direction.

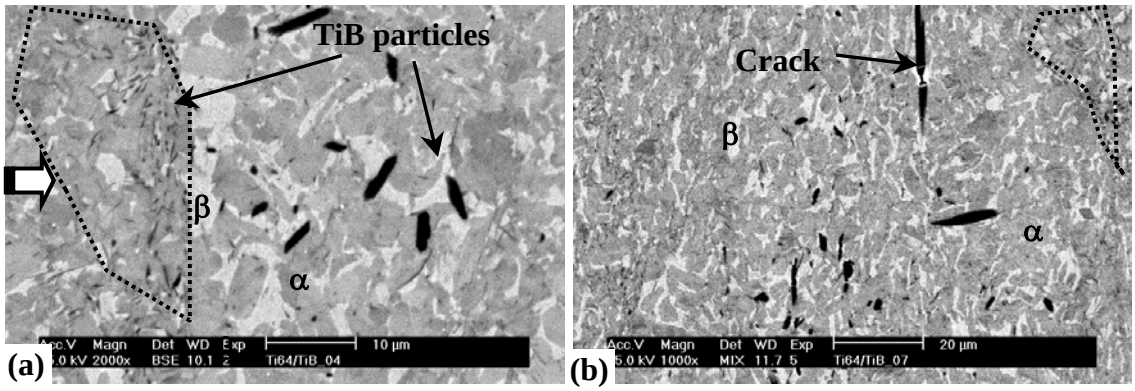

Figure 2: Sample deformed up to 0.3 true strain a) at 850°C and 0.01 s^{-1} showing TiB particles and small TiB needles at the prior β-grain boundaries. A region of small TiB needles is marked by the dotted line. b) at 850°C and 1s^{-1} (BSE) showing a crack in a big TiB particle.

The formation of cracks is observed in the big particles at lower temperatures (Figure 2(b) and Figure 3(a)). At higher temperatures, pores form close to the particles as well as in the matrix, which can be observed in Figure 3(b) and Figure 4(b). The amount of pores and cracks is less than 0.05vol%. A possible explanation for the presence of pores at higher test temperatures in the matrix is that this temperature is higher than the one used in the CHIP production process.

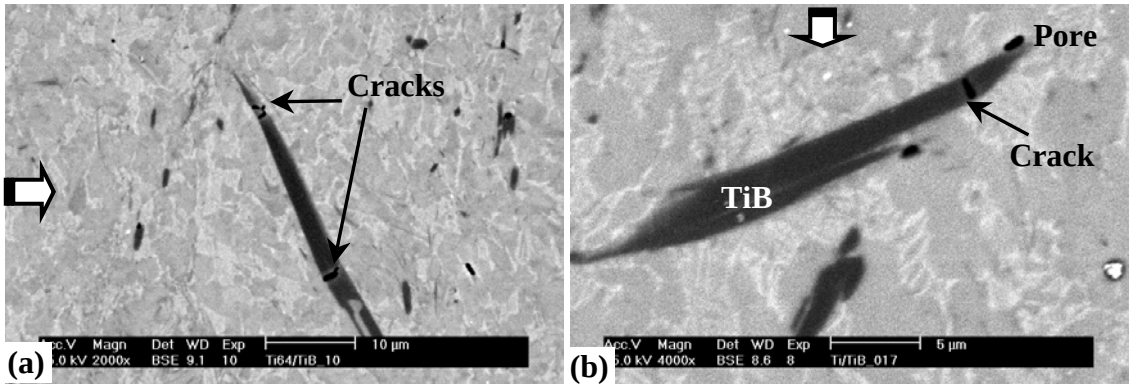

Figure 3: Sample deformed up to 0.3 true strain a) at 900°C and $1s^{-1}$ showing cracks at a big TiB particle b) at 950°C and $1s^{-1}$ (BSE) showing the cracking of TiB, a pore in the matrix near the reinforcement, fine faint α needles in the β–phase in between α grains formed during cooling.

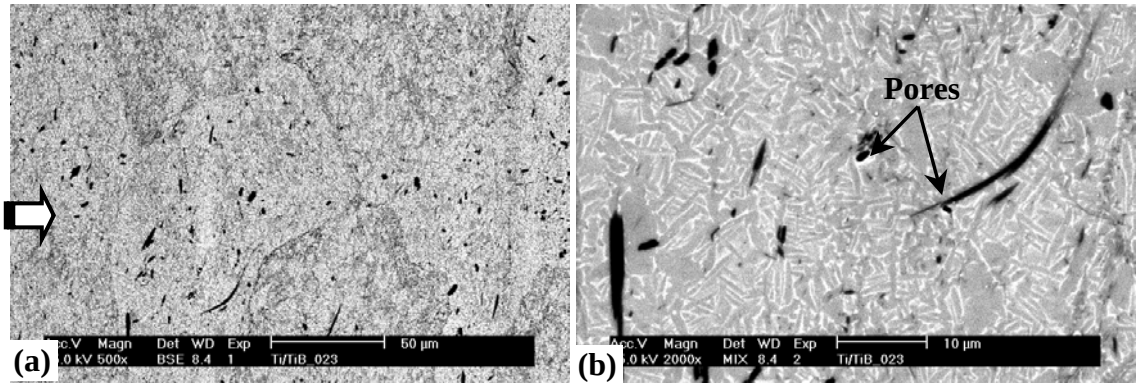

Figure 4 Sample deformed up to 0.3 true strain at 1010°C and $1s^{-1}$ (BSE) showing a) inhomogeneous distribution of TiB particles and b) pores after hot deformation together with small α-grains formed during cooling.

3.2 Deformation behaviour

Figure 5 shows the flow curves up to 0.3 of true strain at strain rates of 0.001-0.1-$10s^{-1}$ for different temperatures.

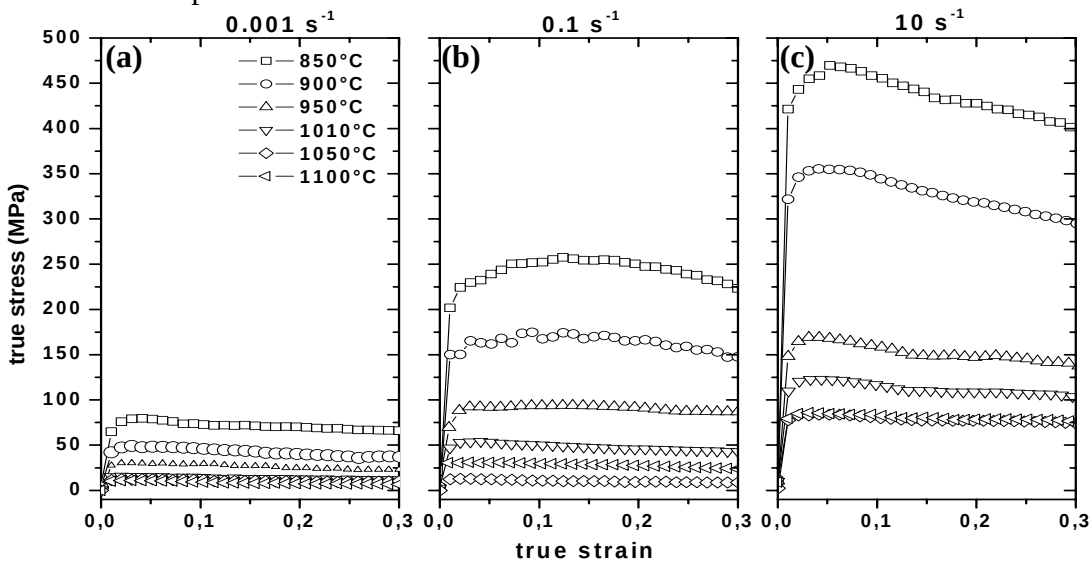

Figure 5: Flow curves at $\dot{\varepsilon}$ of a) $0.001s^{-1}$, b) $0.1\ s^{-1}$ and c) $10\ s^{-1}$ for different test temperatures.

The flow stress increases considerably with increasing strain rate and decreasing temperature.
The overall flow characteristic of Ti-6Al-4V-1.0B-0.1C is summarised in Table 1. On the one hand the described softening can be related to damage caused during the hot deformation process, such as cracks in the particles and/or pore formation in the matrix. On the other hand, it can be caused by flow instability due to flow localization, or due to micro cracking. The oscillations in the flow curves can be related to dynamic recrystallisation or to instabilities in the flow (adiabatic flow). Steady state is related to mechanisms like dynamic recrystallisation, superplasticity or dynamic recovery [18].

Table 1. Flow behaviour of Ti-6Al-4V-1.0B-0.1C at different temperatures and strain rate

Temperature / Strain rate	850°C	900°C	950°C	1010°C	1050°C	1100°C
0.001 s^{-1}	Softening		Steady state			
0.01 s^{-1}	Softening	Flow oscillations	Steady state			
0.1 s^{-1}	Flow oscillations		Steady state			
1 s^{-1}	Softening		Steady state			
10 s^{-1}	Softening			Steady state		

3.3 Processing maps

Comparing the flow stress values obtained from our experiments (accuracy of ±5%) with the measurements of T. Seshacharyulu et. al [19] for Ti64 with lamellar microstructure at 0.3 of true strain, a difference no larger than ±10% is observed indicating no significant hardening effect by the TiB particles.
Using equations 2 and 3 with the flow stress values at a strain of 0.3 determined from the experimental flow curves, the η values were calculated, multiplied by 100 and plotted in a temperature versus strain rate graph in Figure 6. The area of flow instability ($\kappa < 0$), represented by the dashed zone in Figure 6 was determined by calculating the different κ values, using equation 4. S. Tamirisakandala et. al [20] state in their work that the temperature of the beta transus increases with the addition of B by about 60°C, giving a beta transus temperature of approximately 1060°C for this material. The processing map shows high dissipation values above this temperature and at low strain rates for all the temperature under investigation. Flow instabilities are predicted over the whole temperature range when a critical strain is exceeded.
The steady state condition at low strain rates and temperatures between 950 and 1100°C together with the high power dissipation values and the fine grained microstructure suggest the presence of superplasticity, as observed in tension tests in [21] for similar material. The formation of TiB precipitates during material production causes a refinement of the alpha grains, promoting the grain boundary sliding of the soft β phase.
At temperatures below the beta transus and at strain rates higher than $1s^{-1}$, the instability of the material flow can occur as a consequence of the adiabatic flow, which is supported also by the low values of power dissipation and by the observation of an

increment of the temperature of about 1-4% during the compression test. A further reason for the instabilities can be the cracking of reinforcement particles.
The instabilities that occur for all the temperatures and at strain rates between 0.05 and 1 s^{-1} in combination with higher values of power dissipation can be related to the formation of porosity in the matrix during deformation. Above the β-Transus temperature a formation of shear bands can take place. Further, the inhomogeneity in the distribution of the TiB particles causes instabilities on the flow behaviour due to the localization of the material flow.
The grain refinement and the globularization of the alpha phase reduces the internal stresses induced during deformation, decreasing the crack initiation observed in lamellae alpha microstructure [19] and in TiC particle reinforced material [4].

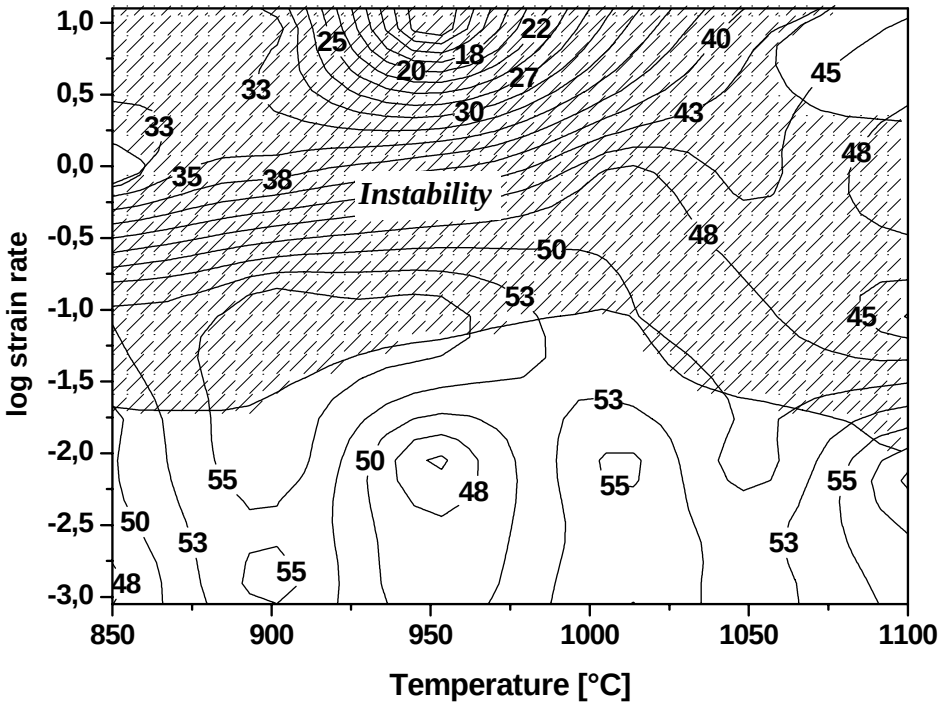

Figure 6: Processing and superimposed instability maps showing isolines of η with high η values at low strain rates.

4 Conclusions

Our studies showed that the reinforcement of Ti 64 by ceramic particles does not only increase the mechanical properties of the material but can also be used to guarantee a fine grained microstructures prior to hot deformation due to the inhibition of grain growth. The precipitation of fine TiB ceramic reinforcements reduces the α-grain size considerably (more than ten times) resulting in an equiaxed alpha microstructure, which reduces the internal stress concentration during hot compression.
During the deformation of Ti-6Al-4V-1.0B-0.1C at high temperatures the formation of cracks and pores (less than 0.4% and smaller than 5µm) adjacent to the precipitates in the α+β field is observed. However, when applying temperatures above β-transus, a breaking of the TiB particles can be avoided.
From the results of this work comparing microstructure, flow curves and processing maps, it can be stated that suitable hot working parameters for this material can be

found at low strain rates and temperatures between 850 and 1100°C and also at high strain rates above the beta transus temperature.

5 Acknowledgments

The authors would like to thank to Dr. Mayer (Inst. of Materials Science and Technology.- Tech University Berlin) for the compression tests at high temperatures and Prof. Degischer (Inst. of Materials Science and Technology.- Tech. University Vienna) for stimulating contributions. The work is partially supported by the Federal Ministry of Economics and Labor in the framework of the Austrian Aeronautic Research (AAR) network

6 References

[1] Luo Guozhen, Zhen Quanpu and Deng Ju. Titanium ’95. III, 2704. **1995.**
[2] M. Peters, C. Leyens: Titan und Titanlegierungen, Wiley VCH, Weinheim **2002.**
[3] Radhaskirshna B. Bhat, Seshacharyulu Tamirisakandala, Dale J. McEldowney, Daniel B. Miracle. ***In press.*** **2003.**
[4] C.Poletti, W. Marketz, H.P Degischer. Ti-2003 Science and Technology. Vol IV. 2531-2538. **2003.**
[5] D.E. Alman, J.A. Hawk. Wear. 225-229.629 **1999.**
[6] P.B. Joshi, G.R. Marathe, N.S.S. Murti, V.K. Kaushik, P. Ramakrishnan. Materials Letters 56. 322–328. **2002.**
[7].V. de Castro, T. Leguey, A. Muñoz, M.A. Monge, R. Pareja Materials Science and Engineering A. ***In press.*** **2005.**
[8] Ke Geng, Weijie Lu, Zhifeng Yang, Di Zhang. Materials Letters 57. 4054–4057. **2003.**
[9] T.W. Clyne, H.M. Flower. Titanium '92. Science and Technology. 2467-2478. **1993.**
[10] H. Feng, O. Meng, Y. Zhou, D. Jia. Materials Science and Engineering . Vol 397. Iss 1-2. 92-97. **2005.**
[11] E. Zhang,, S. Zeng, B. Wang. Journal of Materials Processing Technology. Vol 125-126.- Pages 103-109. **2002**
[12] T.M.T. Godfrey, P.S. Goodwin, C.M. Ward-Close. Titanium '99. Proceedings of the ninth world conference of titanium. Pages 1868-1877. **1999.**
[13] T. Furuta, T. Yamaguchi, Y.Shibata, T. Saito. Titanium '99. Proceedings of the ninth world conference of titanium. Pgs. 1917-1924. **1999.**
[14] S.V.S. Narayana Murty and B. Nageswara Rao. Journal of Materials Science Letters 17. 1203-1205. **1998**
[15] Y.V.R.K. Prasad, H.L. Gegel, S.M. Doraivelu, J.C. Malas, J.T. Morgan, K. A. Lark, D.R. Barker. Metall. Trans. A.15. 1883-1892. **1984**
[16] P. Cavaliere, E. Cerri and P. Leo. Composites Science and Technology. Vol. 64, Iss 9. 1287-1291. **2004**
[17] S.I. Lieberman, A.M. Gokhale, and S. Tamirisakandala. Scripta Materialia. Vol 55, Iss 1. 63-68. **2006**
[18] T. Seshacharyulu, S.C. Medeiros, W.G. Frazier, Y.V.R.K. Prasad. Materials Science and Engineering A284. 184–194. **2000**
[19] T. Seshacharyulu, S.C. Medeiros, W.G. Frazier, Y.V.R.K. Prasad. Materials Science and Engineering A325. 112–125. **2002**
[20] S. Tamirisakandala, R.B. Bhat, D.B. Miracle, S. Boddapati, R. Bordia, R. Vanover, V.K. Vasudevan. Scripta Materialia 53. 217–222. **2005**
[21] Wang Min-min, Lu Wei-jie, Qin Ji-ning, Zhang Di, Ji Bo, Zhu Feng. Scripta Materialia 54. 1955–1959. **2006**